JOURNAL OF GEOPHYSICAL RESEARCH, VOL. 113, D12211, doi:10.1029/2007JD009325, 2008

A study of anthropogenic impacts of the radiation budget and the cloud field in East Asia based on model simulations with GCM

Makiko Mukai,[1] Teruyuki Nakajima,[1] and Toshihiko Takemura[2]

Received 24 August 2007; revised 24 January 2008; accepted 6 February 2008; published 26 June 2008.

[1] We investigated the effects of man-made air pollutants on the climate of East Asia, focusing on eastern China where anthropogenic aerosol concentrations are rapidly increasing. The increasing emission of anthropogenic aerosols causes serious air pollution episodes and various effects on the climate in this region. It is therefore necessary to quantify the contribution of aerosols to the change in the radiation budget and the cloud field. Our purpose of this study is to evaluate the sensitivity of anthropogenic aerosols and other anthropogenic factors such as greenhouse gas (GHG) upon the radiative forcing. Then an aerosol transport model coupled to a general circulation model and an ocean mixed-layer model was used to investigate the relationships among the anthropogenic aerosol forcing, GHG forcing, surface radiation budget, and cloud field. Our simulation results showed that copious anthropogenic aerosol loading causes significant decrease in the surface downward shortwave radiation flux (SDSWRF), which indicates that a direct effect of aerosols has the greatest influence on the surface radiation. It is found from our model simulations that low-level clouds increase but convective clouds decrease due to reduced convective activity caused by surface cooling when anthropogenic aerosol increases, and GHG increase has an insignificant effect on SDSWRF but a significant effect on the cloud field. In other word model simulations suggested that the aerosol forcing mainly causes a reduction of SDSWRF, whereas the change in the cloud field is influenced both anthropogenic aerosol and GHG effects. Thus this work demonstrated with sensitivity experiments the importance of aerosols to cause significant climate effects in the East Asian region, though further study is needed because our study is based on results from one specific model and limited data analysis.

Citation: Mukai, M., T. Nakajima, and T. Takemura (2008), A study of anthropogenic impacts of the radiation budget and the cloud field in East Asia based on model simulations with GCM, *J. Geophys. Res.*, *113*, D12211, doi:10.1029/2007JD009325.

1. Introduction

[2] Asia is the largest and most populous region in the world, in which industrial activity and fossil fuel usage are increasing rapidly [*IEA*, 2004; *REAS*, 2006]. It is well known that the aerosol distributions of Asia are complex due to inhomogeneous emissions of sulfuric, carbonaceous, and other aerosols associated with rapid economic growth and especially fuel burning [*Qian et al.*, 2001; *Tie et al.*, 2005]. The abundance of mineral dust aerosols in this region further complicates the aerosol optical properties [*Nakajima et al.*, 1989, 2003; *Mukai et al.*, 2004].

[3] The global map of the continental haze particle concentration determined from visibility data compiled at surface weather stations also indicates the presence of high concentrations of haze particles around East Asia [*Husar et al.*, 2000; *Luo et al.*, 2001]. Recent MODIS (Moderate Resolution Imaging Spectroradiometer) remote sensing technology has produced detailed and accurate distributions of the aerosol optical thickness (AOT) in eastern China, which is larger than those observed in the eastern United States and Canada, and western Europe [*Chu et al.*, 2003].

[4] The increasing emission of anthropogenic aerosols causes serious air pollution episodes and various effects on the climate in this region by the aerosols interacting with the radiation budget by directly absorbing and scattering the solar radiation [*Charlson et al.*, 1991; *Penner et al.*, 1994], and by them indirectly modifying the optical properties and lifetimes of clouds [*Twomey*, 1974; *Albrecht*, 1989]. Analyses of the observational data show a long-term decreasing trend in the surface downward shortwave radiation flux (SDSWRF) and in the sunshine duration in the last several decades in this region [*Xu*, 2001; *Kaiser and Qian*, 2002; *Liu et al.*, 2004; *Che et al.*, 2005; *Cheng et al.*, 2005; *Hayasaka et al.*, 2006]. Furthermore, data for the clear-sky condition indicate that increased air pollution is mainly responsible for this decreasing trend. However, we see more difficulties in interpreting the decreasing trend in the whole-sky condition because past reports suggested that the cloud coverage also has decreased in this region [*Kaiser* 1998,

[1]Center for Climate System Research, University of Tokyo, Tokyo, Japan.
[2]Research Institute for Applied Mechanics, Kyushu University, Fukuoka, Japan.

0148-0227/08/2007JD009325$09.00

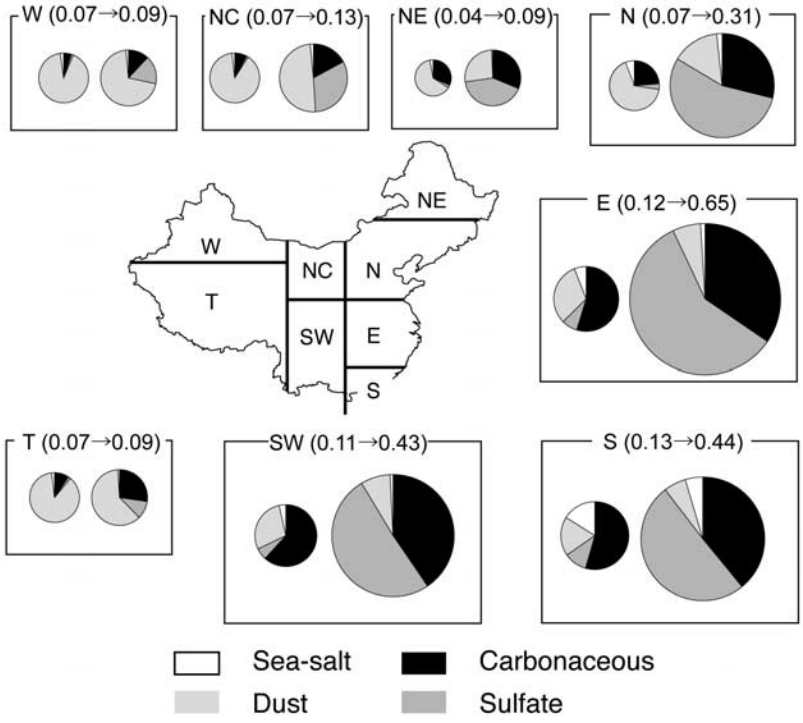

Figure 1. Simulated annual mean aerosol optical thicknesses at 550 nm in eight regions of China as Western China (W): 40–45°N, 75–100°E; Tibet plateau (30–40°N, 75–100°E); Northern central China (NC): 35–45°N, 100–110°E; Southwestern China (SW): 20–35°N, 100–110°E; Southern China (S): 20–25°N, 110–120°E; Eastern China (E): 25–35°N, 110–122°E; Northern China (N): 35–45°N, 110–125°E; Northeastern China (NE): 45–50°N, 110–125°E. Values from experiments using anthropogenic aerosol emission data in the preindustrial (left circles) and in the present-day (right circles).

2000; *Qian et al.*, 2006] which can produce a counter effect of increasing SDSWRF and sunshine duration. It is also necessary to understand why the cloud coverage has decreased in this region despite the strong cloud-lifetime effect caused by air pollution.

[5] Sensitivity experiments based on model simulations are necessary to understand the effects of anthropogenic climate forcing by aerosols and greenhouse gases (GHG) upon the radiation budget and the cloud field of the Asian region, as also suggested by past studies [*Kiehl and Briegleb*, 1993; *Taylor and Penner*, 1994; *IPCC* 2001]. For this purpose we utilize an atmospheric general circulation model (AGCM) with an aerosol transport and radiation model and an ocean mixed-layer model. Also, we focus on eastern China, where available observational data indicate the presence of large anthropogenic emissions.

[6] Our model in this study is described in section 2, and the derived results are analyzed in section 3. The effects of anthropogenic aerosols on the surface radiation budget are presented in section 3.1, and the effects of aerosols and GHG on the cloud field are investigated in sections 3.2 and 3.3. The simulation results are compared with observations in section 4, and conclusions are drawn in section 5.

2. Model

[7] The model in this study was a three-dimensional aerosol transport-radiation model (SPRINTARS; *Takemura et al.* [2000, 2002, 2005]), driven by the AGCM developed by CCSR (Center for Climate System Research), NIES (National Institute for Environmental Studies), and FRCGC (Frontier Research Center for Global Change) [*K-1 Model Developers*, 2004]. The simulated aerosol optical properties are in reasonable agreement with observations. *Takemura et al.* [2002] reported that the mean differences between the simulation and observations are less than 30% for the

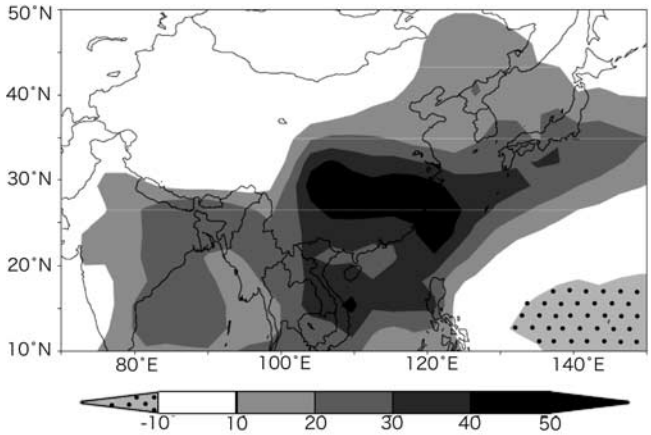

Figure 2. Changes in the annual mean cloud optical thickness. Values represent differences in the simulation results using anthropogenic aerosol emission data between the present-day (2000) and the preindustrial era (1850).

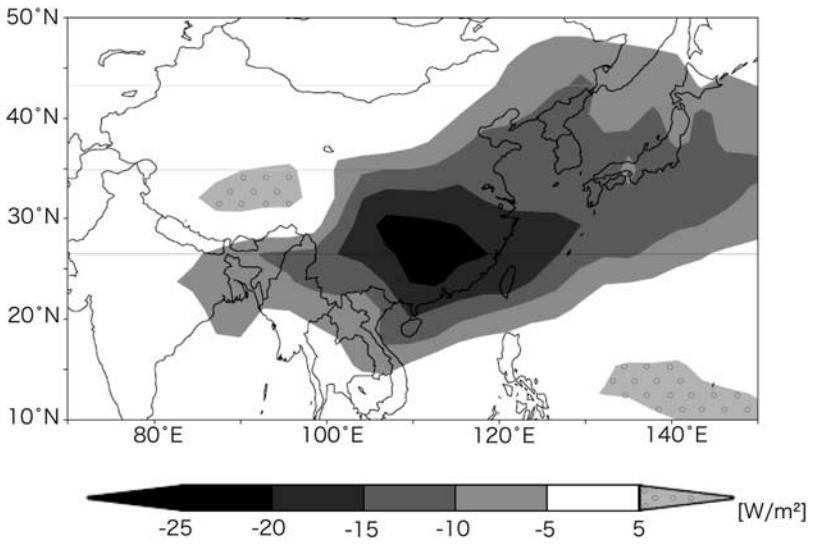

Figure 3. Same as Figure 2 but for the annual mean SDSWRF (W/m^2).

optical thickness in most regions. A simplified mixed-layer ocean was used to simulate the sea surface temperature (SST) change due to aerosols and GHG using the prescribed surface heat flux. The SPRINTARS incorporates sulfate, carbonaceous, sea salt, and mineral dust aerosols, the first three of which are assumed to acts as cloud condensation nuclei that generate cloud droplets whose number increases with the number of nuclei. The effective radius and precipitation rate of cloud droplets were parameterized depending on the number of cloud droplets [*Ghan et al.*, 1997; *Abdul-Razzak et al.*, 1998; *Abdul-Razzak and Ghan*, 2000; *Takemura et al.*, 2005]. The cloud droplet number concentration originating form aerosols is diagnosed as follows:

$$N_c = N_a \times \left[1 + \left\{ f_1(\sigma_a)\left(\frac{AN_a\beta}{3\alpha\omega}\right)^2 + f_2(\sigma_a)\frac{2A^3N_a\beta\sqrt{G}}{27Br_m^3(\alpha\omega)^{3/2}} \right\}^{b(\sigma_a)} \right]^{-1}, \quad (1)$$

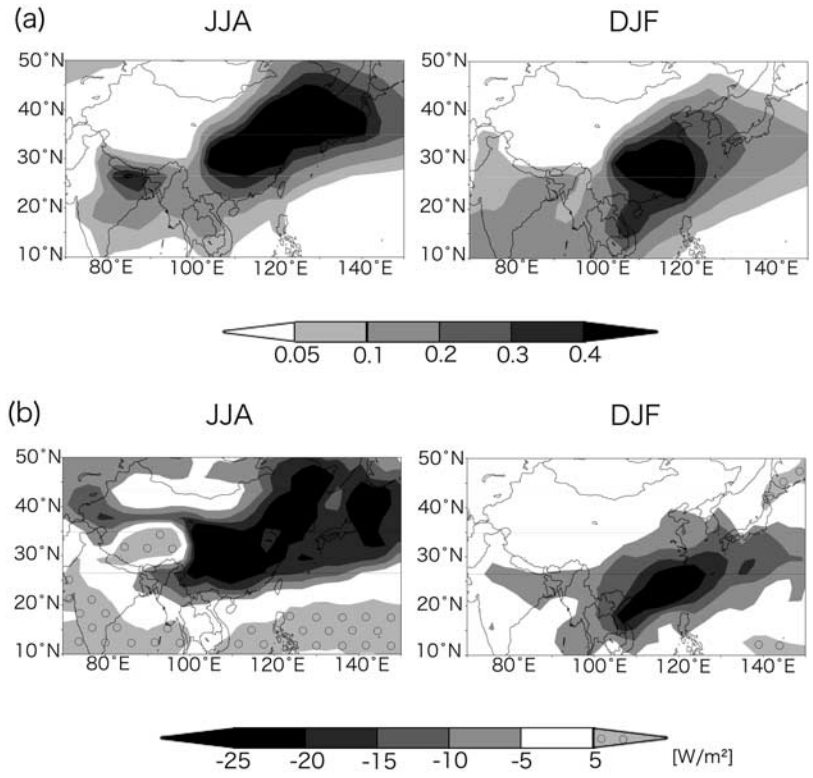

Figure 4. Same as Figure 2 but for summer (June, July, and August; JJA) and winter (December, January, and February; DJF): (a) AOT and (d) SDSWRF (W/m^2).

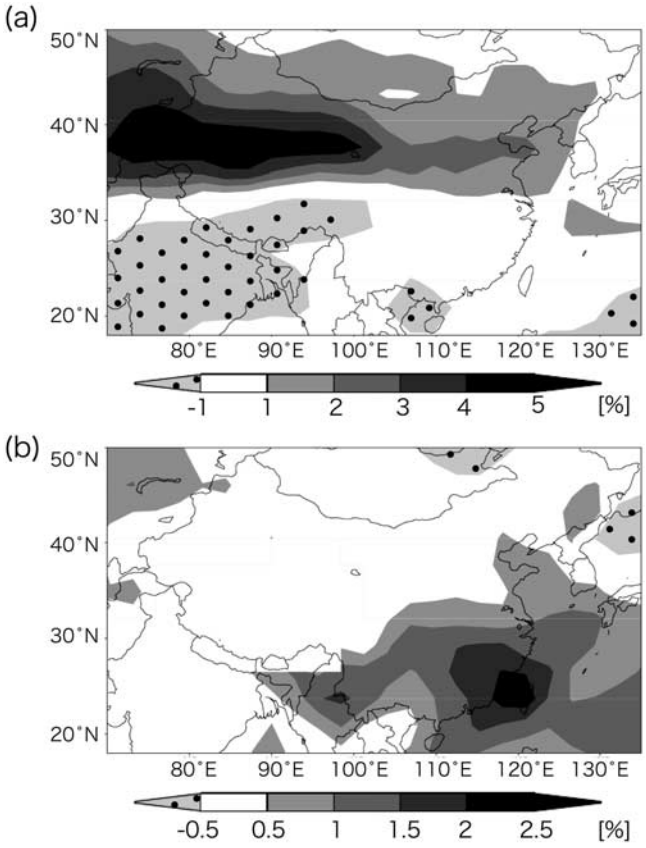

Figure 5. Same as Figure 2 but for the annual mean (a) total cloud coverage and (b) the low-level cloud coverage [%].

where N_c and N_a are cloud droplet and aerosol number concentrations; ω is the updraft velocity; r_m and σ_a are the mode radius and standard deviation of the aerosol particle size distribution; A and B are the coefficients of the curvature and solute effects, respectively; α and β are functions with the saturated water vapor mixing ratio, temperature, and pressure; G is a function with the water vapor diffusivity, saturated water vapor pressure, and temperature; f_1, f_2, and b depend on the standard deviation of the aerosol particle size distribution. The cloud droplet effective radius r_{eff} is then calculated depending N_c as follow:

$$r_{eff} = k\left(\frac{3\rho l}{4\pi\rho_w N_c}\right)^{\frac{1}{3}}, \tag{2}$$

where ρl, ρ_w and k are respectively the air density, cloud water mixing ratio, water density and empirical constant. Then the precipitation rate P is parameterized depending on N_c [*Berry*, 1967] as follows:

$$P = -\frac{dl}{dt} = \frac{\alpha\rho l^2}{\beta + \gamma\frac{N_c}{\rho l}}, \tag{3}$$

where constants are set as $\alpha = 0.01$, $\beta = 0.12$ and $\gamma = 1 \times 10^{-12}$. These parameterizations show that the cloud droplet effective radius decreases (the first indirect effect) with increasing amount of aerosols. A reduced number of particles increases the cloud lifetime and hence decreases the precipitation rate (the second indirect effect). The accuracies of simulated aerosols, cloud, and precipitation fields have already been validated on a global scale using chemical data and AERONET sky radiance data [*Takemura et al.*, 2000, 2002, 2005].

[8] The following three model simulations of equilibrium experiments were performed to investigate the impact of aerosols and GHG based on present-day emission data (represented by 2000) and the preindustrial-era emission data (represented by 1850) provided by *Johns et al.* [2003] and CCSR/NIES/FRCGC [*Nozawa et al.*, 2005]: (Exp. 1) anthropogenic aerosol (sulfate and carbonaceous aerosol from fuel burning) emissions and GHG concentrations for the present-day, (Exp. 2) anthropogenic aerosol emissions for the preindustrial era and GHG concentrations for present-day, and (Exp. 3) anthropogenic aerosol emissions and GHG concentrations for the preindustrial era. We assumed no emissions of carbonaceous aerosols and sulfate aerosol originating from fossil fuels for the preindustrial era and emissions of carbonaceous aerosol originating from biofuel and agricultural activities for the preindustrial era to be about a tenth of that for the present-day. The same emissions database of volcanic SO_2 from continuous eruptions, carbonaceous aerosol from biomass burning, and the terpene emitted from plants as one of the OC were used in all experiments. Each experiment required integration for at least 20 years before equilibrium was reached, with the subsequent 30 years being investigated. The anthropogenic-aerosols impact (AI), GHG impact (GI), and total anthropogenic impact (including both anthropogenic aerosols and GHG; AGI) were evaluated from the differences between Exp. 1 and Exp. 2, Exp. 2 and Exp. 3, and Exp. 1 and Exp. 3, respectively. So, these simulations indicate the results of sensitivity test.

3. Results

3.1. Aerosol Effects on the Surface Radiation Budget

[9] Figure 1 presents simulated annual mean AOT at a wavelength of 550 nm for eight regions of China in the experiment using anthropogenic aerosol emission data in the preindustrial (left circles) and the experiment using anthropogenic aerosol emission data in the present-day (right circles). The pie chart in each panel shows contributions of aerosol types in each period, with the circle diameter corresponding to the total amount of aerosols (on an arbitrary scale). It is found that the simulated aerosol concentrations in the present-day in eastern and southern produce an annual mean AOT with contributions of 90% from sulfate and carbonaceous aerosols, and less than 10% from dust and sea salt aerosols. The dominance of anthropogenic components such as sulfate and carbonaceous aerosols in these regions is consistent with the presence of heavy industrial activity and fuel burning [*Chu et al.*, 2003; *Akimoto et al.*, 2006]. In contrast, the annual mean total AOT was less than 0.1 over eastern China in the preindustrial era. Figure 1 indicates that the total AOT increased four- to fivefold from the preindustrial era to the present-day, with a tendency of increase getting greater at locations

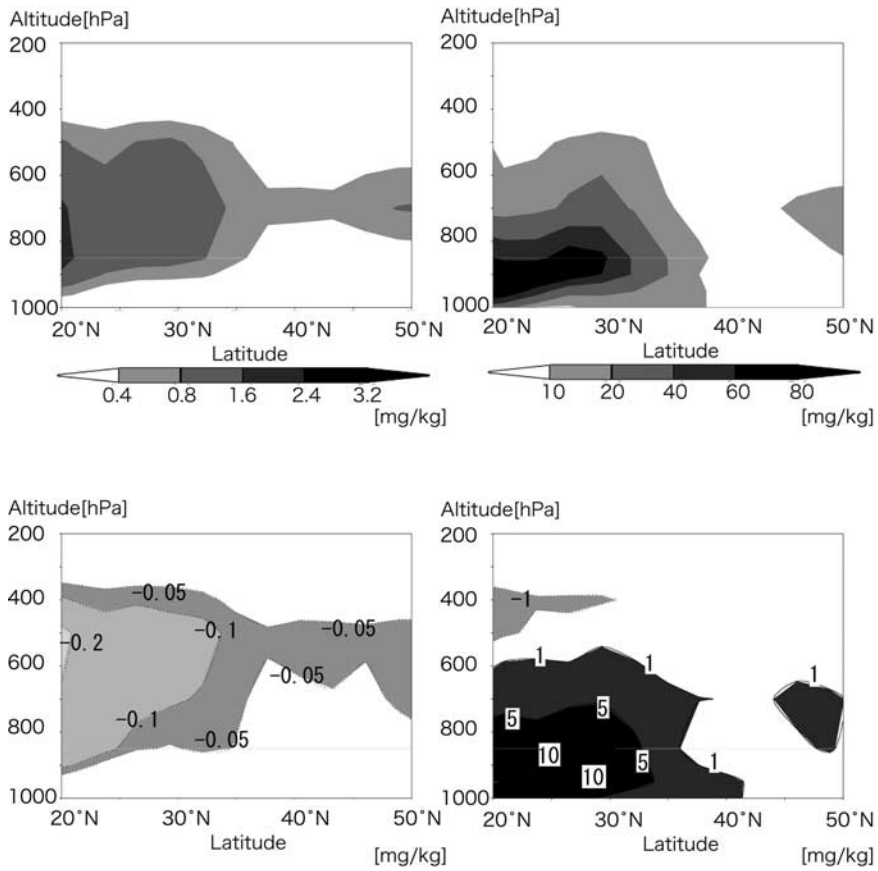

Figure 6. Vertical distributions of annual mean cloud water concentrations (mg/kg) averaged over 110–120°E. Top panels represent the result of the control run, and bottom panels are the same as for Figure 2. Left and right panels represent convective cloud and large-scale condensation cloud, respectively.

nearer to sources of the aerosol sources in eastern China, caused primarily by increases in sulfate and carbonaceous aerosols associated with fuel burning. This increase in the aerosol loading causes changes in the number of cloud droplets and hence in the cloud optical thickness, as shown in Figure 2 over a wide area from eastern China to Japan. This figure shows that the change in the cloud optical thickness reaches 40 near the main source of aerosol emissions. Note that the distribution of the cloud change differs slightly from that of the AOT change shown in Figure 1, which indicates that the cloud-field change is caused not only by aerosol indirect effects but also by other mechanisms as described in section 3.2. The SDSWRF-change field shown in Figure 3 reflects all the changes in AOT and cloud optical thickness shown in Figures 1 and 2. It also depends on the cloud coverage change as shown in Figure 5 as discussed later. Figure 3 shows that SDSWRF decreases by 15 W/m^2 over the large area of eastern China as is shifted to the oceanic region as compared with the AOT-change field.

[10] Figure 4 indicates that the changes in AOT and SDSWRF show significant seasonal variation between summer (June, July, and August) and winter (December, January, and February). The region of large AOT extends from southwestern to northeastern China and to Japan in summer, whereas the enhanced AOT is limited to near the source area in winter. It should be noted that anthropogenic aerosol emissions from source areas were assumed to be constant (i.e., without seasonal variation) in the model simulations. The significant seasonal change in AOT must therefore be due to variations in the photochemical reaction process and transportation process. Photochemical reactions are active in summer, with more sulfate aerosols produced from SO_2, while aerosol particle generation is modest in winter near the source region. Furthermore, aerosol particles are lifted to higher altitudes in summer than in winter, which allows them to be transported farther and with a longer residential time in summer. Similar to the seasonal difference in the AOT-change distribution, the area of reduced SDSWRF is larger in summer than in winter as shown in Figure 4b. The simulated seasonal difference in the AOT-change field is supported by the AOT distributions derived from the TERRA/MODIS satellite imager, which also shows a wider AOT distribution in summer [*Chu et al.*, 2003]. However, there are noticeable differences between SDSWRF and AOT-change distributions that are more distinct than those in the annual mean distributions in Figures 1 and 3. Although not shown in a figure, this difference is caused by the cloud-coverage-change field differing from the AOT-change field. A wide region from eastern to northeastern China is covered with thick clouds in the model simulation in summer. Additionally, the cloud-coverage maximum over China occurs in summer [*Li et al.*,

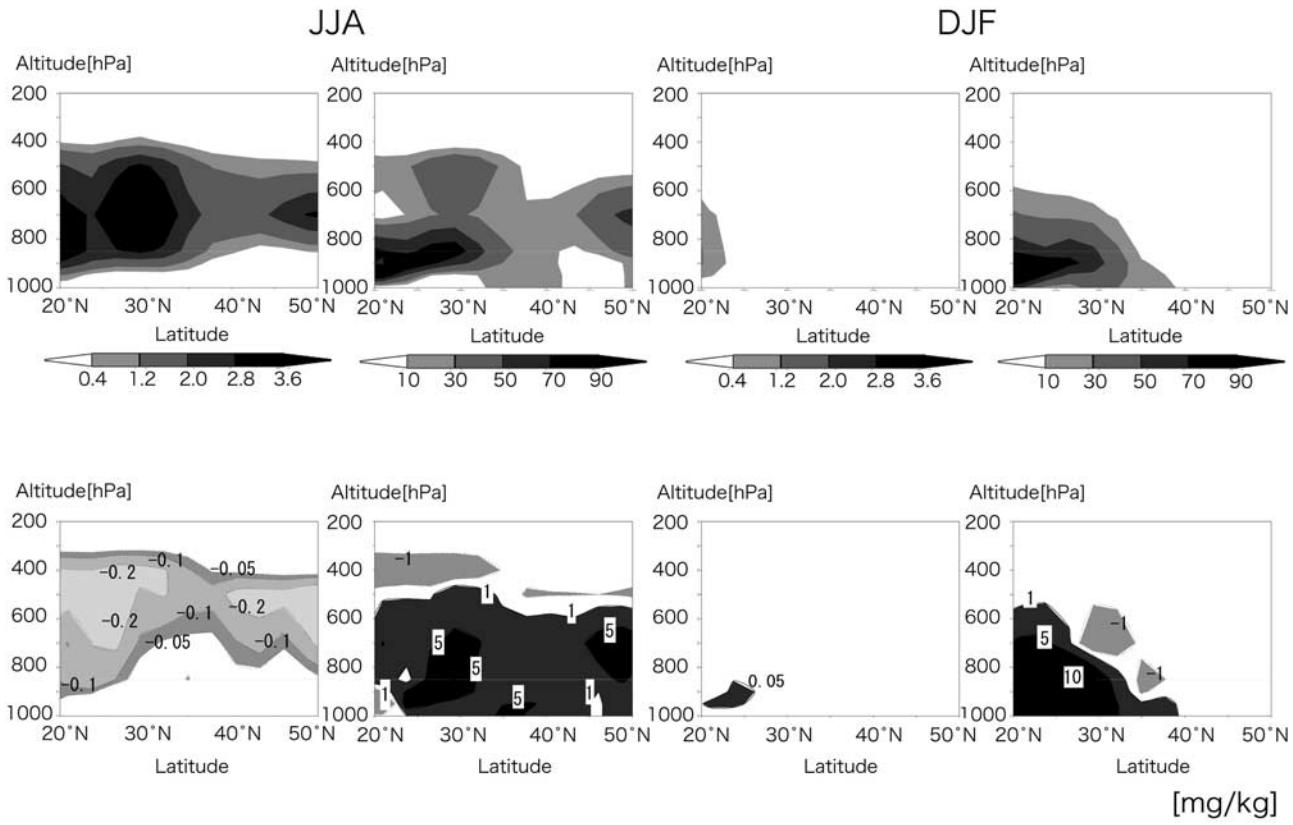

Figure 7. Same as Figure 6 but for the averaged values over summer (JJA) and winter (DJF).

2004]. This enhancement in the cloud optical thickness and coverage further decreases SDSWRF in this region.

3.2. Cloud Field Change by Aerosol Effects

[11] The previous section indicates that the aerosol loading results in complicated changes in the cloud coverage. In this section we consider how cloud changes are produced. Figure 5 indicates the change in the coverage of total and low-level cloud (under 680 hPa). The low-level cloud coverage increases with the concentration of anthropogenic aerosols, as explained by an enhanced indirect (cloud lifetime) effect caused by the increase in anthropogenic aerosols. The cloud droplet number concentration increases by the aerosol number concentration increase and precipitation rate decrease shown in equations (1) and (3). This feature appears clearly in the vertical distribution of clouds in Figure 6, which presents the annual mean vertical distribution of the cloud water concentration change induced by AI averaged over eastern China from 110°E to 120°E. The large-scale condensation-cloud water increases in the lower atmosphere around the area where anthropogenic aerosol emissions increase (Figure 6b). However, the change in the total cloud coverage differs from that for low-level cloud. In our model the aerosol second indirect effect is treated only in large-scale condensation clouds. Therefore the convective-cloud water decrease evident in the figure appears to be caused by mechanisms other than the aerosol first and second indirect effects. Figure 7 is the same as Figure 6 except that it shows the summer and winter averages. The decrease in the convective-cloud water is clear in summer, but there is very little convective-cloud water in winter over China.

[12] A candidate mechanism is the weaker convection flow caused by the surface cooling due to an increase in aerosols, especially in summer as shown in Figure 8a. This figure shows the change in winds during summer when anthropogenic aerosols increase (i.e., AI). An increase in aerosols causes surface cooling by reducing SDSWRF, especially from northeastern China to Japan in summer. The updraft flow in this region becomes weaker due to strong surface cooling and stronger downdraft flow in central China. Moreover, the change in 850-hPa winds weakens the characteristic southwesterly winds blowing from the west coast of India. This suggests that the eastern Asian summer monsoon circulation is attenuated by AI. This trend agrees with the result of *Iwasaki and Kitagawa* [1998] reporting that a lower low-level temperature due to an aerosol increase weakens the summer monsoon circulation, which decreases the total cloud coverage in summer over southern China due to weaker convective activity. On the other hand, the large-scale condensation cloud dominates in winter and the cloud coverage change pattern becomes similar to that of the aerosol increase because of the dominance of aerosol indirect effects.

[13] Table 1 indicates the seasonal change in total and low-level cloud coverage in the following climatic regions as defined by *Liu et al.* [2004]: northern China defined as the region including Beijing (35–45°N, 110–125°E), eastern China the region in the mid-to-lower reaches of the Yangtze River (25–35°N, 110–122°E), and southern China

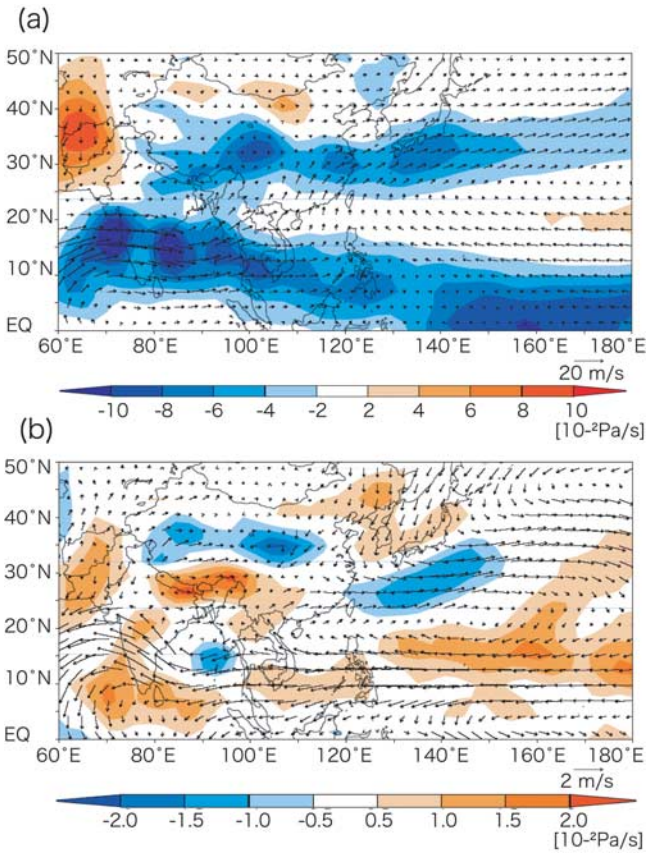

Figure 8. Pressure velocity (10^{-2} Pa/s) at 400 hPa (shadow) and wind vector (m/s) at 850 hPa (vectors) in summer for the control run (upper panel) and the simulated change induced by AI (lower panel).

which is the region south of 25°N (20–25°N, 110–120°E). The low-level cloud coverage increases in almost all seasons in all the regions, especially in southern and eastern China during winter. This characteristic spatial and seasonal dependence is mainly caused by the aerosol indirect effect due to large anthropogenic emissions in these areas. On the other hand, the total cloud coverage decreases in southern and eastern China from summer to autumn, which is mainly due to surface cooling caused by the significant decrease in SDSWRF.

3.3. Cloud Field Change by GHG Effects

[14] The climate forcing by greenhouse gases is greatly different from that by the anthropogenic aerosols. Also, hence the simulated results are different from each other increasing greenhouse gases warm the surface while increasing aerosols cool the surface. Therefore the change in the cloud coverage induced by increases in greenhouse gas differs from that in aerosols. Changes in the seasonal and annual mean values of the cloud coverage induced by increases in GHG in the three regions are shown in Table 1. The low-level cloud coverage tends to decrease when GHG increase in all the regions, although the magnitude of the change is smaller than that induced by aerosols. The change in the total cloud coverage induced by increases in GHG is almost the opposite of that due to the aerosol increase. When GHG increases, the annual mean cloud coverage decreases in northern and eastern China. This fact is seemed to be at least partially induced by decreases in the relative humidity as shown in Figure 9 which presents the vertical distribution of the annual mean relative humidity for the change induced by GI averaged over (110–120°E) in the region (20–50°N).

[15] However, from summer to autumn, the total cloud coverage increases over southern and eastern China with the enhancement of high-level clouds. This seasonal change in the total cloud coverage is connected to the change in the East Asian monsoon circulation due to the increase in GHG, such as a stronger summer monsoon as also proposed by *Kimoto* [2005].

4. Comparison With Observations

[16] In this section we compare the model simulation results presented in the preceding sections with observed changes in the cloud coverage and SDSWRF. *Kaiser* [1998] reported that the trend in the annual mean midday cloud coverage during 1951–1994 was −1.0% per decade in eastern China. In order to compare our simulation results with this observed long-term change, Figure 10 indicates

Table 1. Seasonal and Annual Mean Changes in Total Cloud Coverage (%) and Low-Level (Under 680 hPa) Cloud Coverage (%) Induced by AI and GI Averaged Over Each Region in China[a]

			MAM	JJA	SON	DJF	YR
AI	total cloud coverage	N	1.3	3.2	1.3	0.9	1.7
		E	3.0	0.5	−2.2	1.8	0.8
		S	1.6	−1.3	−4.4	1.9	−0.5
	low-level cloud coverage	N	0.1	0.6	0.3	0.1	0.3
		E	2.0	0.4	−0.2	2.7	1.2
		S	1.5	0.4	0.9	3.2	1.5
GI	total cloud coverage	N	−1.1	−4.0	−2.0	0.8	−1.6
		E	−3.6	1.0	0.3	−4.2	−1.6
		S	−1.3	3.6	5.6	−0.2	1.9
	low-level cloud coverage	N	0.2	−0.1	−0.2	0.1	0.0
		E	−0.6	0.3	−0.4	−0.7	−0.4
		S	0.0	−0.5	−1.0	−1.8	−0.8

[a]Northern China (N: 35–45°N, 110–125°E), Eastern China (E: 25–35°N, 110–122°E) and Southern China (S: 20–25°N, 110–120°E) for the spring season (MAM: March, April, and May) and the fall season (SON: September, October, and November), respectively.

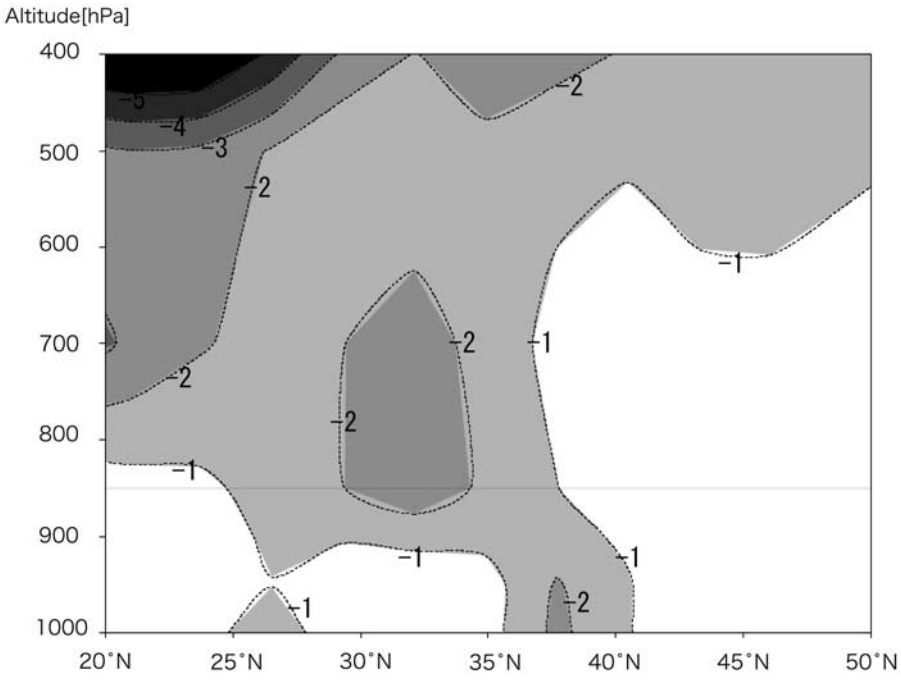

Figure 9. Vertical distribution of annual mean relative humidity (%) averaged over 110–120°E for the simulated change induced by GI.

changes in the model results induced by AI, GI, and AGI, and surface-observed trends of the annual mean cloud coverage [*Kaiser*, 1998] in the same three regions as in Table 1. As also shown in Table 1, the annual mean total cloud coverage increases from a negative to a positive value with increasing latitude from south to north due to a larger decrease in the high-level clouds in southern regions, especially in summer. In contrast, the annual mean total cloud coverage decreases in northern and eastern China induced by GI. The cloud coverage increases in southern China due to a significant increase in high-level clouds. These AI- and GI-induced changes in cloud coverage compensate each other so as to reduce the magnitude of the total cloud coverage change induced by both factors (AGI). Thus the annual mean cloud coverage increases by about 1.3% in southern China, decreases by about 0.8% in eastern China, and does not change in northern China. On the other hand, most stations in China show statistically significant decreases in the cloud coverage. These observed trends are less consistent with the modeled trends in the three regions. However, it should be noted that the simulated change in cloud coverage induced by GI is more inconsistent with the observed trend. Inclusion of AI brings the simulated cloud coverage change trend closer to the observed trend. The high-level cloud coverage change due to SST change, as discussed in the previous section, is especially important in AI. Inclusion of only the aerosol indirect effect, which increases the low-level clouds, makes the simulation results less consistent with the observed trend. It should be remembered that our simulation results are from equilibrium experiments, which tend to overestimate the impacts, and which may at least partially explain the differences between the observed and simulated results.

[17] Figure 11 compares between observed and simulated SDSWRF changes at the following sites in China: Lanzhou (36.63°N, 103.53°E) in north-central China, Shenyang (41.44°N, 123.27°E) and Beijing (39.56°N, 116.17°E) in northern China, Chengdu (30.4°N, 104.01°E) in southwestern China, Wuhan (30.37°N, 114.08°E) in eastern China, and Guangzhou (23.08°N, 113.09°E) in southern China. The black dots in the figure indicate the measured SDSWRF change trend from 1961 to 2000 in China provided by the China Meteorological Administration. The observations indicate a decreasing trend in SDSWRF, with the value reaching more than -20 W/m^2 in industrial areas over the 40 years at all sites. Figure 11 indicates that the model simulation is consistent with the site dependence of the observed trends, though the absolute values from the

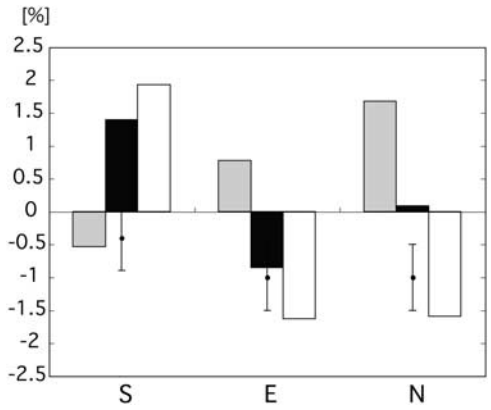

Figure 10. Changes in the annual mean cloud coverage (%) in the same three regions as in Table 1. Hatched, dark grey, and open bars indicate simulated changes induced by AI, AGI, and GI, respectively. Black dots represent the changes in the observed cloud coverage (%) from 1951 to 1994 and bars indicate standard errors.

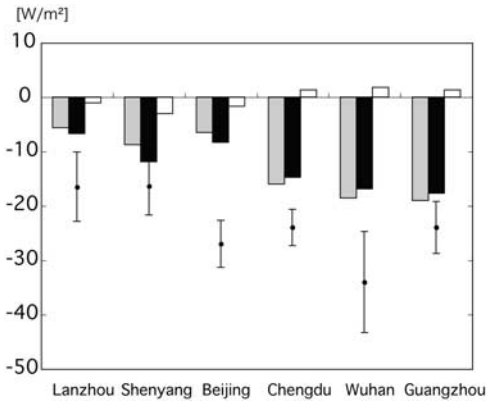

Figure 11. Same as Figure 10 but for the simulated annual mean SDSWRF (W/m^2) at six sites in China: Lanzhou (36.63°N, 103.53°E), Shenyang (41.44°N, 123.27°E), Beijing (39.56°N, 116.17°E), Chengdu (30.4°N, 104.01°E), Wuhan (30.37°N, 114.08°E), and Guangzhou (23.08°N, 113.09°E). Hatched, dark grey, and open bars indicate simulated changes induced by AI, AGI, and GI, respectively. Black dots represent the changes in annual mean observed SDSWRF (W/m^2) from 1961 to 2000 and bars indicate standard errors.

simulation underestimate the observed trend by 30–50%. It should again be noted again that the model simulations are equilibrium experiments, which would be expected to be different from the values obtained in transient experiments. We therefore conclude that our model underestimates the observed negative trends of SDSWRF, and future studies should be attempted to identify the underlying reason for this discrepancy. One possible reason is an underestimation of the emission inventory near large cities, because the spatial resolution of our emission inventory is of order of 100 km. The other point to be recognized in the figure is that aerosol effects are the dominant factor changing the SDSWRF at all the sites in China without significant GI effects as also indicated in the earlier sections. The GHG influence on the SDSWRF is mostly caused through changes in the cloud coverage, because the AOT changes little over China when GHG increased in our simulations.

[18] Figure 12 shows the annual mean SDSWRF in the three regions in China due to each factor. The aerosol direct effect is the main contributor to the change in SDSWRF in the clear-sky condition, while the aerosol indirect effect is the main factor to cause the difference in the SDSWRF change in the whole sky from that in clear sky. It is found that the AI is mostly due to direct effects. On the other hand, aerosol indirect effects vary between regions. It should be noted that the indirect effects in our study include not only ordinary aerosol indirect effects but also general circulation effects. It is found in this study that the change in the radiation budget due to the aerosol direct effect and the first and second indirect effects cause a change in the land and ocean surface temperature by which a secondary atmospheric general circulation is induced. Thus the SDSWRF change as well as the cloud field change is very intricate and the magnitude of aerosol indirect effects is different from region to region. For instance, such a region covered with a large cloud amount is susceptible to changes indicated in this figure.

5. Conclusions

[19] Present sensitivity study using model simulations has revealed the complicated effects of anthropogenic aerosols on the climate in China. In our simulations the AOT values increase by about fivefold over eastern China relative to the preindustrial era. The observations show a significant negative change in SDSWRF (of more than −20 W/m^2) over the last 40 years, due mostly to the direct effect of aerosols, and this has been confirmed by our model simulations. Furthermore, we found that the change in the aerosol distribution varies with seasons, which causes the seasonal changes in AOT, cloud properties, and SDSWRF.

[20] In our model simulations when anthropogenic aerosols increase, the low-level cloud coverage increases in all seasons but the total cloud coverage decreases in summer, especially over southern China. This decrease appears to be due to reduced convective activity caused by surface cooling. The annual mean cloud coverage over eastern China

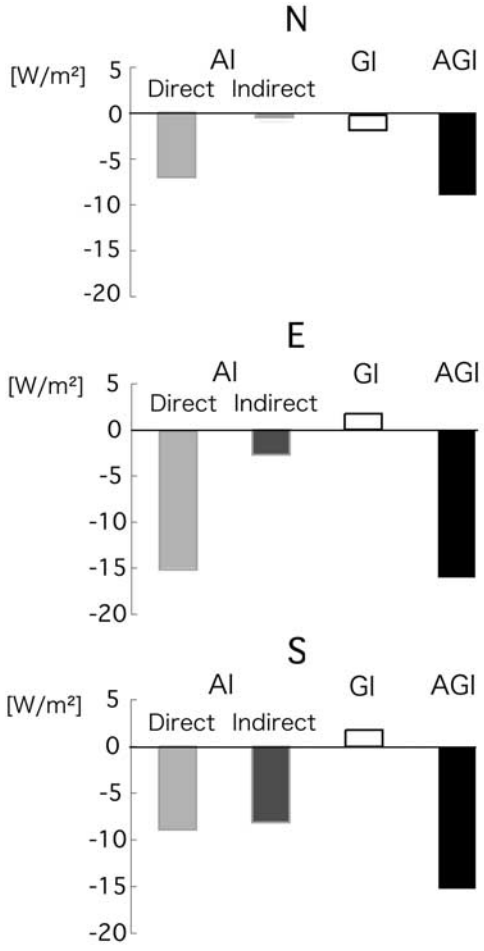

Figure 12. Same as Figure 11 but for the annual mean SDSWRF (W/m^2) in northern, eastern, and southern China. AI (direct) indicates change in SDSWRF (clear sky), and AI (indirect) indicates SDSWRF (whole sky) − SDSWRF (clear sky).

increases with the marked increase in low-level clouds due to increasing aerosols. On the other hand, low-level cloud coverage decreases when GHG increase, and the total cloud coverage also decreases except in the summer, especially over southern China. The annual mean cloud coverage decreases over northern and eastern China and increases over southern China induced by GI. The observed decrease in the cloud coverage in China [*Kaiser*, 1998; *Kaiser and Qian*, 2002; *Qian et al.*, 2006] needs both the effects of aerosols and GHG to be included in the model simulation.

[21] Since the above findings have been drawn in this study based on a specific model and limited data analysis, we need more studies of comprehensive simulations with variety of models to validate against more observational data in order to accurately explain the observed trends in the radiation budget and the cloud field. Especially detailed transient simulations based on fine resolution emission inventories of aerosols will be important to study the disagreement between observed and simulated SDSWRF. It is also needed to study model dependence of the cloud field change due to the induced general circulation caused by GHG and aerosol increase with various models including full-coupled atmosphere and ocean models. However, it is possible to say that at least the present sensitivity experiments demonstrate a large potential of aerosols to interpret the observed trends in SDSWRF and cloud coverage in this region.

[22] **Acknowledgments.** We thank developers of the AGCM at the CCSR, NIES, and FRCGC; T. Nozawa (National Institute of Environmental Studies) for providing the historical emission data; T. Hayasaka (Research Institute for Humanity and Nature) and G. Shi (Chinese Academy of Sciences) for providing the surface observation data for China; and the Japan meteorological business support center for making available other data used in this study. Makiko Mukai thanks the staff members at the CCSR for their helpful discussions and encouragement, and also N. Schutgens for his great help with her English. The simulations were performed on the NEC SX-6 supercomputer at the NIES. This research was supported by Global Environment Research Fund B-4 of the Ministry of Environment, Japan; the RR2002 project and the data integration for Earth observation project of the Ministry of Science, Sports, and Culture; and the JAXA/ADEOS-II GLI project.

References

Abdul-Razzak, H., and S. J. Ghan (2000), A parameterization of aerosol activation: 2. Multiple aerosol type, *J. Geophys. Res.*, *105*, 6837–6844.

Abdul-Razzak, H., S. J. Ghan, and C. Rivera-Carpio (1998), A parameterization of aerosol activation: 1. Single aerosol type, *J. Geophys. Res.*, *103*, 6123–6131.

Akimoto, H., T. Ohara, J. Kurokawa, and N. Hori (2006), Verification of energy consumption in China during 1996–2003 by using satellite observational data, *Atmos. Environ.*, *40*, 7663–7667.

Albrecht, B. A. (1989), Aerosol, cloud microphysics, and fractional cloudiness, *Science*, *245*, 1227–1230.

Berry, E. X. (1967), Cloud droplet growth by collection, *J. Atmos. Sci.*, *24*, 688–701.

Charlson, R. J., J. Langner, H. Rodhe, C. B. Leovy, and S. G. Warren (1991), Perturbation of the Northern Hemisphere radiative balance by back-scattering from anthropogenic aerosol, *Tellus, Ser. A and Ser. B*, *43*, 152–163.

Che, H. Z., G. Y. Shi, X. Y. Zhang, R. Arimoto, J. Q. Zhao, L. Xu, B. Wang, and Z. H. Chen (2005), Analysis of 40 years of solar radiation data from China, 1961–2000, *Geophys. Res. Lett.*, *32*, L06803, doi:10.1029/2004GL022322.

Cheng, Y. J., U. Lohmann, J. H. Zhang, Y. F. Luo, Z. T. Liu, and G. Lesins (2005), Contribution of changes in sea surface temperature and aerosol loading to the decreasing precipitation trend in southern China, *J. Clim.*, *18*(9), 1381–1390.

Chu, D. A., Y. J. Kaufman, G. Zibordi, J. D. Chern, J. Mao, C. Li, and B. N. Holben (2003), Global monitoring of air pollution over land from the Earth Observing System-Terra Moderate Resolution Imaging Spectroradiometer (MODIS), *J. Geophys. Res.*, *108*(D21), 4661, doi:10.1029/2002JD003179.

Ghan, S. J., L. R. Leung, R. C. Easter, and A. Abdul-Razzak (1997), Prediction of cloud droplet number in a general circulation model, *J. Geophys. Res.*, *102*, 21,777–21,794.

Hayasaka, T., S. Hayashida, T. Iwami, K. Kawamoto, T. Nakajima, T. Nakazawa, T. Saeki, and G. Shi (2006), Emissions of greenhouse gases and aerosols, and human activities in the eastern Asia, http://www.chikyu.ac.jp/Project2-1

Husar, R. B., J. D. Husar, and M. Laurent (2000), Distribution of continental surface aerosol extinction based on visual range data, *Atmos. Environ.*, *34*, 5067–5078.

IEA (International Energy Agency) (2004), Key World Energy Statistic, report, Paris, France.

Intergovernmental Panel on Climate Change (IPCC) (2001), Contribution of working group 1 to the third assessment report, in *Climate Change 2001: The Scientific Basis*, edited by J. T. Houghton et al., p. 881, Cambridge Univ. Press, New York.

Iwasaki, T., and H. Kitagawa (1998), A possible link of aerosol and cloud radiations to Asian summer monsoon and its implication in long-range numerical weather prediction, *J. Meteorol. Soc. Jpn.*, *76*, 965–982.

Johns, T. C., et al. (2003), Anthropogenic climate change for 1860 to 2100 simulated with the HadCM3 model under updated emission scenarios, *Clim. Dyn.*, *20*, 583–612.

K-1 Model Developers (2004), K-1 coupled GCM (MIROC) description, edited by H. Hasumi and S. Emori, *K-1 Tech. Rep., 1*, 34 pp., Cent. for Clim. Syst. Res., Univ. of Tokyo, Tokyo.

Kaiser, D. P. (1998), Analysis of total cloud amount over China, 1951–1994, *Geophys. Res. Lett.*, *25*, 3599–3602.

Kaiser, D. P. (2000), Decreasing cloudiness over China: An updated analysis examining additional variables, *Geophys. Res. Lett.*, *27*, 2193–2196.

Kaiser, D. P., and Y. Qian (2002), Decreasing trends in sunshine duration over China for 1954–1998: Indication of increased haze pollution?, *Geophys. Res. Lett.*, *29*(21), 2042, doi:10.1029/2002GL016057.

Kiehl, J. T., and B. P. Briegleb (1993), The relative roles of sulfate aerosols and greenhouse gases in climate forcing, *Science*, *260*, 311–314.

Kimoto, M. (2005), Simulated change of the east Asian circulation under global warming scenario, *Geophys. Res. Lett.*, *32*, L16701, doi:10.1029/2005GL023383.

Li, Y. Y., R. C. Yu, Y. P. Xu, and X. H. Zhang (2004), Spatial distribution and seasonal variation of cloud over China based on ISCCP data and surface observations, *J. Meteorol. Soc. Jpn.*, *82*, 761–773.

Liu, B., M. Xu, M. Henderson, and W. Gong (2004), A spatial analysis of pan evaporation trends in China, 1955–2000, *J. Geophys. Res.*, *109*, D15102, doi:10.1029/2004JD004511.

Luo, Y., D. Lu, X. Zhou, W. Li, and Q. He (2001), Characteristics of the spatial distribution and yearly variation of aerosol optical depth over China in last 30 years, *J. Geophys. Res.*, *106*(D13), 14,501–14,513.

Mukai, M., T. Nakajima, and T. Takemura (2004), A study of long-term trends in mineral dust aerosol distributions in Asia using a general circulation mode, *J. Geophys. Res.*, *109*, D19204, doi:10.1029/2003JD004270.

Nakajima, T., M. Tanaka, M. Yamano, M. Shiobara, K. Arao, and Y. Nakanishi (1989), Aerosol optical characteristics in the yellow sand events observed in May, 1982 in Nagasaki - Part II Model, *J. Meteorol. Soc. Jpn.*, *67*, 279–291.

Nakajima, T., et al. (2003), Significance of direct and indirect radiative forcings of aerosols in the East China Sea region, *J. Geophys. Res.*, *108*(D23), 8658, doi:10.1029/2002JD003261.

Nozawa, T., T. Nagashima, H. Shiogama, and S. A. Crooks (2005), Detecting natural influence on surface air temperature change in the early twentieth century, *Geophys. Res. Lett.*, *32*, L20719, doi:10.1029/2005GL023540.

Penner, J. E., R. J. Charlson, J. M. Hales, N. S. Laulainen, R. Leifer, T. Novakov, J. Ogren, L. F. Radke, S. E. Schwartz, and L. Travis (1994), Quantifying and minimizing uncertainty of climate forcing by anthropogenic aerosols, *Bull. Am. Meteorol. Soc.*, *75*, 375–400.

Qian, Y., F. Giorgi, Y. Huang, W. L. Chameides, and C. Luo (2001), Regional simulation of anthropogenic sulfur over east Asia and its sensitivity to model parameters, *Tellus, Ser. B*, *53*, 171–191.

Qian, Y., D. P. Kaiser, L. R. Leung, and M. Xu (2006), More frequent cloud-free sky and less surface solar radiation in China from 1955 to 2000, *Geophys. Res. Lett.*, *33*, L01812, doi:10.1029/2005GL024586.

REAS (Regional Emission Inventory in Asia) (2006), http://www.jamstec.go.jp/frcgc/research/d4/emission.htm, Frontier Research Center for Global Change, Japan Agency for Marine-Earth Science and Technology.

Takemura, T., H. Okamoto, Y. Maruyama, A. Numaguti, A. Higurashi, and T. Nakajima (2000), Global three-dimensional simulation of aerosol optical thickness distribution of various origin, *J. Geophys. Res.*, *105*, 17,853–17,873.

Takemura, T., T. Nakajima, O. Dubovik, B. N. Holben, and S. Kinne (2002), Single-scattering albedo and radiative forcing of various aerosol species with a global three-dimensional model, *J. Clim.*, *15*, 333–352.

Takemura, T., T. Nozawa, S. Emori, T. Y. Nakajima, and T. Nakajima (2005), Simulation of climate response to aerosol direct and indirect effects with aerosol transport-radiation model, *J. Geophys. Res.*, *110*, D02202, doi:10.1029/2004JD005029.

Taylor, K. E., and J. E. Penner (1994), Response of the climate system to atmospheric aerosols and greenhouse gases, *Nature*, *369*, 734–737.

Tie, X., S. Madronich, S. Walters, D. P. Edwards, P. Ginoux, N. Mahowald, R. Zhang, C. Lou, and G. Brasseur (2005), Assessment of the global impact of aerosols on tropospheric oxidants, *J. Geophys. Res.*, *110*, D03204, doi:10.1029/2004JD005359.

Twomey, S. (1974), Pollution and the planetary albedo, *Atmos. Environ.*, *8*, 1251–1256.

Xu, Q. (2001), Abrupt change of the mid-summer climate in central east China by the influence of atmospheric pollution, *Atmos. Environ.*, *35*, 5029–5040.

M. Mukai and T. Nakajima, Center for Climate System Research, University of Tokyo, 5-1-5 Kashiwanoha, Kashiwa, Chiba 277-8568, Japan. (mukai@ccsr.u-tokyo.ac.jp)

T. Takemura, Research Institute for Applied Mechanics, Kyushu University, 6-1 Kasuga-koen, Kasuga, Fukuoka 816-8580, Japan.